Hindawi
Shock and Vibration
Volume 2021, Article ID 6617609, 17 pages
https://doi.org/10.1155/2021/6617609

Research Article

Analysis of Influence of Stress Lode Angle on Stability of Roadway Surrounding Rock

Yihong Liu,[1,2] Hongbao Zhao ,[1,2] Lei Wang,[1] Tao Wang,[2] Dongliang Ji,[2] and Rui Liu[2]

[1]*State Key Laboratory of Mining Response and Disaster Prevention and Control in Deep Coal Mines, Anhui University of Science and Technology, Huainan, Anhui 232001, China*
[2]*School of Energy and Mining Engineering, China University of Mining & Technology-Beijing, Beijing 100083, China*

Correspondence should be addressed to Hongbao Zhao; hongbaozhaovip@163.com

Received 17 December 2020; Revised 4 January 2021; Accepted 24 January 2021; Published 8 February 2021

Academic Editor: Gong-Da Wang

Based on the variation range of the stress lode angle, the in situ rock stress is divided into σ_v-type stress field, σ_H-type stress field, and σ_h-type stress field. Through theoretical analysis, the principal stress difference distribution law and plastic zone distribution pattern around the roadway in different types of stress fields are obtained. Theoretical and numerical simulation calculation results show that under different stress lode angle conditions, the principal stress difference distribution of the surrounding rock of the roadway is greatly different, which has a direct effect on the shape and range of the plastic zone of the surrounding rock of the roadway. In the σ_v-type stress field and the σ_H-type stress field, the shape of the plastic zone of the roadway surrounding rock is mainly oval and "butterfly," while in the σ_h-type stress field, the shape of the plastic zone of the roadway surrounding rock is mainly oval. The laboratory test proves that the stress gradient has an important effect on the damage degree of the surrounding rock of the roadway. The larger the stress gradient, the higher the strength of the rock mass and the more severe the damage. The change of the stress lode angle will affect the distribution law of the stress gradient of the surrounding rock of the roadway, thus affecting the degree of fragmentation of the surrounding rock. In type σ_v and type σ_H stress fields, the surrounding rock of the shoulder can be regarded as a key part of the roadway. In the σ_h-type stress field, the plastic zones of the surrounding rocks of the roadway are more evenly distributed, and the damage range is less affected by θ. The influence law of the stress lode angle on the stability of the roadway has been well verified by field observation, and effective support measures have been proposed.

1. Introduction

In-situ stress is the fundamental force that causes instability and damage in underground construction projects and is also an important basis for the design of various underground excavation projects [1, 2]. The distribution characteristics and deformation characteristics of the plastic zone of the surrounding rock have an obvious stress correlation. A large number of scholars have used theoretical analysis, numerical simulation, engineering practice, and other methods to study the effects of stress environment on the failure of surrounding rock in the roadway or round hole. The research results are abundant [3–7]: revealing the principal stress difference and plastic zone response characteristics of surrounding rock of gob-side entry in deep mine [8], influence of lateral pressure coefficient and the angle of the axial and maximum principal stress on the stability of roadway [9], the rupture range of the surrounding rock of the roadway under different initial stresses [10], and the influence of the initial in-situ stress on the blasting crack under the action of the explosion stress wave [11]. At present, according to the roadway geology and production conditions, a variety of roadway surrounding rock control technologies have been developed [12] support, reinforcement, stress control, joint support, and other methods to solve a large number of roadway support problems.

In the actual in-situ environment, the three principal stress values of the in-situ rock stress are not equal in most cases [13], and most scholars treat the two

horizontal stresses to be approximately equal or take gravity stress or tectonic stress as a separate influencing factor to study its influence on roadway stability. A large number of studies have shown that the three principal stress changes and the combination relations of the three principal stresses have an important impact on the instability of the rock mass [14, 15]. The stress lode angle, as a stress state parameter that reflects the relationship between the three principal stresses, can not only reflect the change of the principal stress amplitude but also the change of the stress principal axis. Therefore, the stress lode angle is used to characterize the stress environment of the surrounding rock of the roadway in this paper. The influence of the changes of the stress lode angle on the stability of the surrounding rock of the roadway is studied. It is found that the distribution law of principal stress difference affects the plastic zone range and plastic zone morphology of surrounding rock of roadway, and the stress gradient affects the fracture scale and dimension of surrounding rock. Therefore, the principal stress difference and stress gradient were used as the medium to study the influence mechanism of the stress lode angle on the stability of the surrounding rock of the roadway. In the existing research, the influence of the distribution of the three principal stresses on the roadway support design is rarely considered. Therefore, this paper studies the instability characteristics of roadway surrounding rock under different stress lode angle conditions, puts forward the key points and key areas of roadway support under different stress field conditions, and verifies the research results on-site, in order to bring new ideas for roadway support design.

1.1. Theoretical Analysis of Influence of Stress Lode Angle on the Stress Field of Surrounding Rock of Roadway. Underground structures such as roadways and chambers are often in a triaxial stress environment. The changes of the three principal stresses and the deflection of the stress principal axis can cause different degrees of damage to the underground structures [16, 17]. The stress lode angle can reflect the relationship between the three principal stresses [18, 19]. This article uses the stress lode angle to characterize the stress environment of the surrounding rock of the roadway. Assume that the horizontal stress σ_H perpendicular to the axial direction of the roadway, the horizontal stress σ_h parallel to the axial direction of the roadway, and the vertical stress σ_v are three principal stresses, respectively. The relationship between each principal stress and the stress lode angle is as follows:

$$\begin{Bmatrix} \sigma_H \\ \sigma_h \\ \sigma_v \end{Bmatrix} = \begin{Bmatrix} p \\ p \\ p \end{Bmatrix} + \frac{2\sqrt{3J_2}}{3} \begin{Bmatrix} \sin\left(\theta + \frac{2}{3}\pi\right) \\ \sin\theta \\ \sin\left(\theta - \frac{2}{3}\pi\right) \end{Bmatrix}, \tag{1}$$

$$p = \frac{1}{3}(\sigma_1 + \sigma_2 + \sigma_3), \tag{2}$$

$$J_2 = \frac{1}{6}\left[(\sigma_1 - \sigma_2)^2 + (\sigma_2 - \sigma_3)^2 + (\sigma_3 - \sigma_1)^2\right], \tag{3}$$

where p is spherical stress; J_2 is the second invariant of the deviatoric stress; θ is stress lode angle; σ_1, σ_2, and σ_3 are, respectively, the maximum, intermediate, and minimum principal stresses in the original rock stress.

This paper mainly studies the influence of the stress lode angle on the stability of the surrounding rock of the roadway. Therefore, the spherical stress and the second invariant of the deviatoric stress are set to a fixed value. Combined with the actually measured data of the in-situ stress of the coal mine of the cases in section 5, let $p = 15$ MPa and $J_2 = 48$ MPa^2. The range of the stress lode angle is -30°~310°, and the interval is 20°. A total of 18 loading schemes are obtained. Figure 1(a) shows the law of changes of the three principal stresses with the stress lode angles. It can be seen from Figure 1(a) that the position of the principal stress axis changes once every 60 degrees of the stress lode angle, thereby six principal stress space partitions were obtained, as shown in Figure 1(b).

Based on the law of changes of the minimum principal stress, the stress environment shown in Figure 1 is divided into the following three types of in-situ stress fields: the σ_v type stress field, that is, the vertical principal stress is the minimum principal stress, and the stress lode angle range is -30°~90°; the σ_H type stress field, that is, the horizontal stress perpendicular to the axial direction of the roadway is the minimum principal stress, and the stress lode angle range is 90°~210°; the σ_h type stress field, that is, the horizontal stress parallel to the axial direction of the roadway is the minimum principal stress and stress lode angles range from 210° to 330°.

1.2. Distribution Characteristics of Main Stress Difference of Surrounding Rock in Circular Roadway. When the properties of the surrounding rock are constant, the change of stress state is the main factor for the instability of the surrounding rock of the roadway or chamber. The effect of the stress lode angle on the stability of the surrounding rock

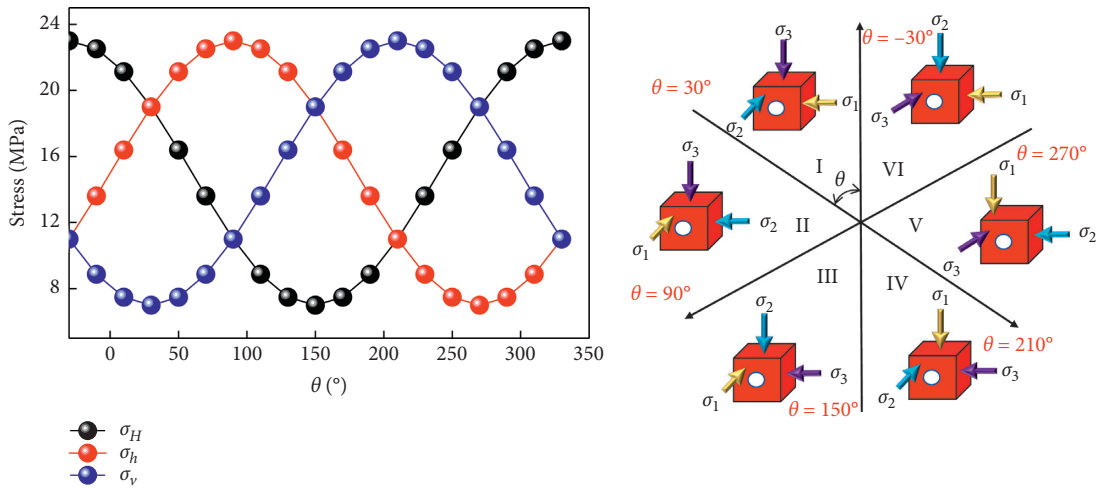

(a) (b)

FIGURE 1: Stress loading and principal stress spatial distribution. (a) Relationship between principal stress and stress lode angle. (b) Stress state distribution map.

of the roadway is mainly reflected in the change of the surrounding rock stress state. From the generalized plane strain theory, the relationship between the radial stress, tangential stress, and shear stress of the roadway (round hole) with respect to the far-field stress of the surrounding rock and the roadway radius is as follows [20]:

$$\left.\begin{aligned}
\sigma_r &= \frac{1}{2}(\sigma_v + \sigma_H)\left(1 - \frac{R_0^2}{r^2}\right) - \frac{1}{2}(\sigma_v - \sigma_H)\left(1 - 4\frac{R_0^2}{r^2} + 3\frac{R_0^4}{r^4}\right)\cos 2\alpha,\\
\sigma_\theta &= \frac{1}{2}(\sigma_v + \sigma_H)\left(1 + \frac{R_0^2}{r^2}\right) + \frac{1}{2}(\sigma_v - \sigma_H)\left(1 + 3\frac{R_0^4}{r^4}\right)\cos 2\alpha,\\
\sigma_z &= \sigma_h - 2\mu(\sigma_H - \sigma_v)\frac{R^2}{r^2}\cos 2\alpha,\\
\tau_{r\theta} &= \frac{1}{2}(\sigma_H - \sigma_v)\left(1 + 2\frac{R_0^2}{r^2} - 3\frac{R_0^4}{r^4}\right)\sin 2\alpha,\\
\tau_{z\theta} &= 0,\\
\tau_{rz} &= 0,
\end{aligned}\right\} \quad (4)$$

where α is the polar angle; R_0 is the radius of the roadway; r is any position of the roadway surrounding rock.

In the rectangular coordinate system, the stress of each point of the surrounding rock of the roadway can be converted as follows:

$$\sigma_x = \sigma_r \cos^2(\alpha) + \sigma_\theta \sin^2(\alpha) - 2\tau_{r\theta}\sin(\alpha)\cos(\alpha),$$

$$\sigma_y = \sigma_r \sin^2(\alpha) + \sigma_\theta \cos^2(\alpha) - 2\tau_{r\theta}\sin(\alpha)\cos(\alpha),$$

$$\sigma_z = \sigma_h - 2\mu(\sigma_H - \sigma_v)\frac{R^2}{r^2}\cos\ 2\ \alpha,$$

$$\tau_{xy} = (\sigma_r - \sigma_\theta)\sin(\alpha)\cos(\alpha) + \tau_{r\theta}\left(\cos^2(\alpha) - \ \sin^2(\alpha)\right). \tag{5}$$

The one-dimensional cubic stress state characteristic equation for solving principal stress in elasticity is shown in equation (6), and its three real roots σ_1', σ_2', and σ_3' are three principal stresses.

$$\sigma^3 - I_1\sigma^2 + I_2\sigma - I_3 = 0. \tag{6}$$

In the formula,

$$\left.\begin{aligned} I_1 &= \sigma_x + \sigma_y + \sigma_z, \\ I_2 &= \sigma_x\sigma_y + \sigma_y\sigma_z + \sigma_z\sigma_x - \tau_{xy}^2 - \tau_{yz}^2 - \tau_{zx}^2, \\ I_3 &= \sigma_x\sigma_y\sigma_z + 2\tau_{xy}\tau_{yz}\tau_{zx} - \sigma_x\tau_{yz}^2 - \sigma_y\tau_{zx}^2 - \sigma_z\tau_{xy}^2. \end{aligned}\right\} \tag{7}$$

Three roots that can be obtained based on the complex operation formula as follows:

$$\left.\begin{aligned} \sigma_1' &= \frac{I_1}{3} + 2\sqrt{-\frac{p'}{3}}\cos\left(\frac{\theta'}{3}\right), \\ \sigma_2' &= \frac{I_1}{3} \sqrt{-\frac{p'}{3}}\left(\cos\left(\frac{\theta'}{3}\right) - \sqrt{3}\ \sin\left(\frac{\theta'}{3}\right)\right), \\ \sigma_3' &= \frac{I_1}{3} - \sqrt{-\frac{p'}{3}}\left(\cos\left(\frac{\theta'}{3}\right) + \sqrt{3}\ \sin\left(\frac{\theta'}{3}\right)\right). \end{aligned}\right\} \tag{8}$$

In the formula,

$$\left.\begin{aligned} \theta' &= \arccos\left[-\frac{q}{2}\left(-\frac{(p')^3}{27}\right)^{-(1/2)}\right] \quad (0 \le \theta' \le \pi), \\ p' &= \frac{3I_2 - I_1^2}{3}, \\ q &= \frac{9I_1I_2 - 2I_1^2 - 27I_3}{27}. \end{aligned}\right\} \tag{9}$$

The principal stress difference can that indirectly reflect the distribution of the shear stress is the elastoplastic characterization of the material under arbitrary loads [21, 22]. The principal stress difference is equal to the maximum principal stress minus the minimum principal stress, that is,

$$\sigma_s = \left|\sigma_1' - \sigma_3'\right|. \tag{10}$$

From the formulas (1) to (10), the principal stress difference distribution of the surrounding rock under different stress lode angles in three stress fields can be obtained. Let $R_0 = 2.5$ m and use Matlab calculation software to get the distribution map of the principal stress difference of the surrounding rock of the roadway, as shown in Figure 2.

It can be seen from Figure 2 that, in the σ_v type stress field, the principal stress difference between the shoulder corner and the bottom corner of the roadway is large. When the stress lode angle is −30~30°, there is a large concentration range of the principal stress difference, which indicates the stability of the surrounding rock of the roadway is poor, and when the stress lode angle is 50~70°, the concentration range of the principal stress difference is small, and the stability of the surrounding rock of the roadway is relatively good; in the σ_H-type stress field, when the stress lode angle is 90~130°, the concentration range of the main stress difference is small and the surrounding rock is relatively stable. When the stress lode angle is 150~190°, the concentration range of the main stress difference is large, so the stability of surrounding rock is poor; in the σ_h-type stress field, compared with the σ_H-type stress field and the σ_v-type stress field, the principal stress difference concentration range of the surrounding rock of the roadway is generally smaller, and there is no large-scale concentration phenomenon of the principal stress difference at the shoulder and bottom corners of the roadway, and the stability of the surrounding rock of the roadway is relatively good.

1.3. Boundary Morphology of Roadway Surrounding Rock Plastic Zone. Regarding the calculation of the boundary of the plastic zone of the surrounding rock of a circular roadway under two-way or three-way unequal pressure conditions, no precise analytical solution has been given so far. Assuming that the surrounding rock is still in an elastic state after the excavation of the roadway, the stress of the surrounding rock after the excavation based on the elastic theory can be substituted into the plastic equation to determine the elastic-plastic boundary, although this solution is only an approximate solution, for engineering, the error of this approximate solution is acceptable. Mohr–Coulomb criterion is currently the most mature, most widely used, and recognized rock failure criterion in geotechnical engineering. Compared with other rock failure criteria, this failure criterion has the advantages of fewer parameters, simple application, and easy understanding. According to the Mohr–Coulomb strength criterion, when the rock mass is in the limit equilibrium state, the relationship between the maximum and minimum principal stresses satisfies the following relationship:

$$F = \sigma_1' - 2C\frac{\cos\varphi}{1 - \sin\varphi} - \frac{1 + \sin\varphi}{1 - \sin\varphi}\sigma_3' = 0, \tag{11}$$

where C is cohesion, MPa; φ is friction, °. According to the above formula, when $F = 0$ means that the surrounding rock of the roadway is at the critical point of elasticity and

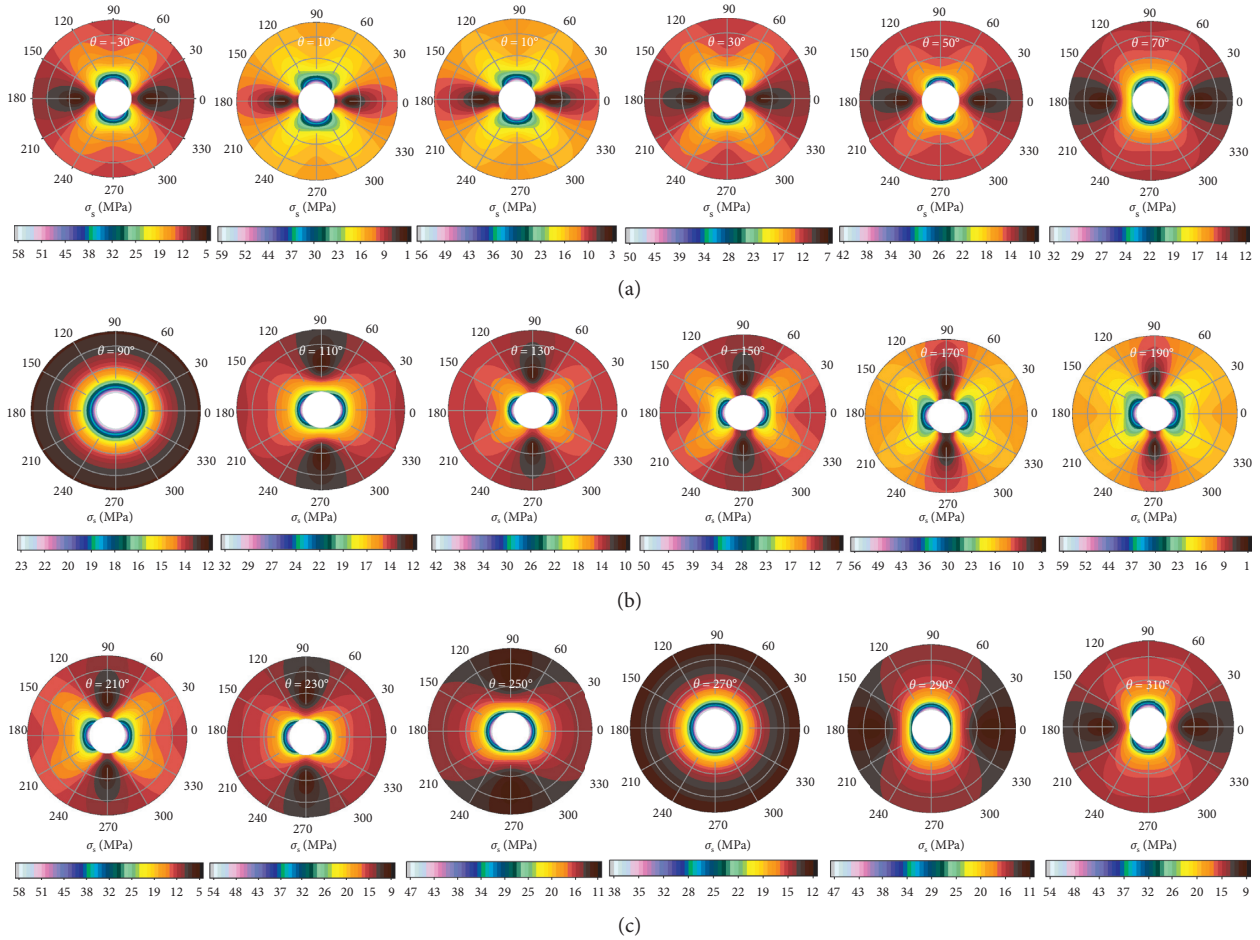

FIGURE 2: Distribution of principal stress difference of surrounding rock in different types of stress fields. (a) σ_v-type stress field. (b) σ_H-type stress field. (c) σ_h-type stress field.

plasticity, if $F > 0$, it means that the rock mass has entered the plastic state. According to the engineering geological data and coal seam mechanical parameters of Huipodi Coal Mine, let C be 2.2 MPa and φ be 23°. From the formulas (8) and (11), the distribution characteristics of the boundary line between the elastic zone and the plastic zone of the roadway surrounding rock under different stress lode angles are obtained, as shown in Figure 3.

It can be seen from Figure 3 that the boundary shape of the plastic zone of the surrounding rock of the roadway under different stress lode angles is mainly circular, oval, and "butterfly". In the σ_v-type stress field and the σ_H-type stress field, the shape and range of the plastic zone of the surrounding rock of the roadway are greatly affected by the stress lode. However, in the σ_h-type stress field, the boundary shape of the plastic zone is mainly elliptical and the shape and range do not change much under different stress lode angle conditions. Compared with the σ_v-type stress field and the σ_H-type stress field, the plastic zone of the surrounding rock of the roadway in the σ_h-type stress field is smaller, and the stability of the surrounding rock is better. Comparing Figure 2, it can be seen that the boundary shape of the plastic zone of the surrounding rock of the roadway under different stress lode angle conditions is similar to the distribution pattern of the concentration range of the principal stress difference, which also proves that the distribution of the principal stress difference has an important effect on the stability of the surrounding rock of the roadway.

2. Numerical Simulation Results

It can be seen from the analyses in section 1 that the change of the stress lode angle can directly lead to the change of the distribution of the principal stress difference of the surrounding rock of the roadway, which in turn affects the stability of the surrounding rock of the roadway. In this section, numerical simulation is used to verify the influence of the change of the stress lode angle on the distribution of principal stress difference of roadway surrounding rock and the stability of surrounding rock. The model was established based on the actual geological conditions of the roadway involved in the case study in section 5. The calculation range of the model is 40 m * 40 m * 10 m, the roadway size is 4.4 m * 3.2 m, and the number of grids in the model is 250,000. The horizontal and vertical displacements of the model are limited to the side and the bottom, respectively. The thickness of each rock layer and its physical and mechanical parameters are shown in Table 1. The calculation

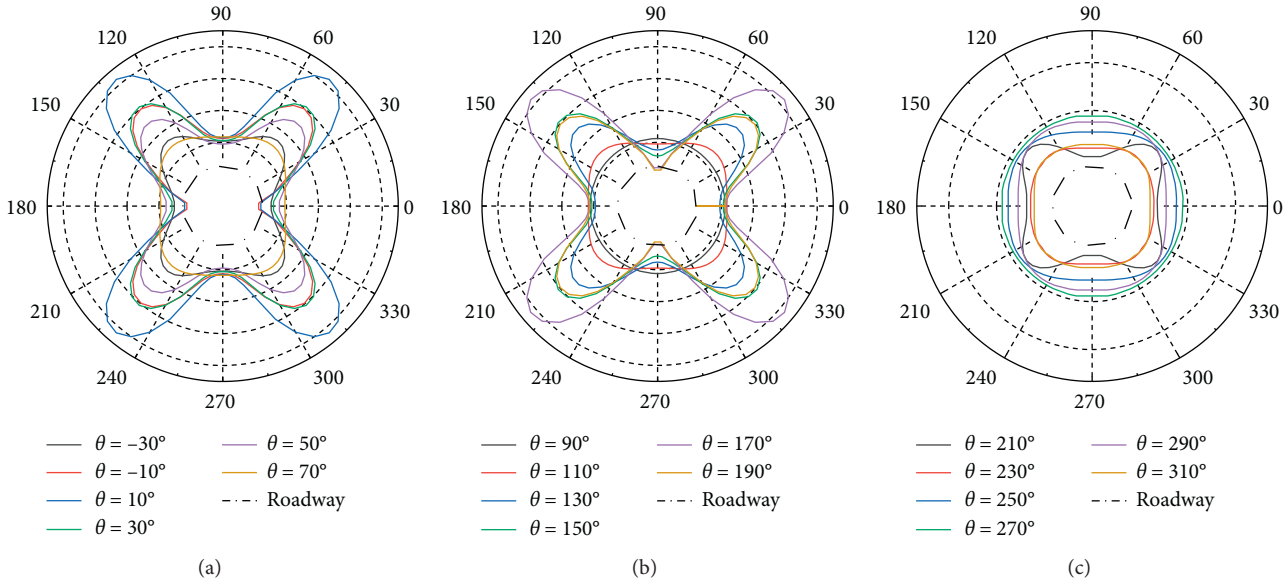

Figure 3: Distribution of the boundary line of the surrounding rock plastic zone. (a) σ_v type stress field. (b) σ_H type stress field. (c) σ_h type stress field.

Table 1: Rock physical and mechanical parameters table.

Strata	Thickness (m)	Density (kg m^{-3})	Bulk modulus (GPa)	Shear modulus (GPa)	Cohesion (MPa)	Tensile strength (MPa)	Friction (°)
Upper rock mass	6	2600	8.82	4.63	4.0	2.6	34
Mudstone	4	2570	13.4	7.5	2.5	1.8	32
10# coal seam	2.4	2570	13.4	7.5	1.8	1.8	32
Siltstone	2.4	2580	3.3	2.5	1.6	1.3	25
Mudstone	4	2461	6.08	3.47	1.7	1.3	25.5
11# coal seam	3.2	2620	7.52	3.1	1.9	1.2	26
Mudstone	4.4	2660	5.7	3.4	1.8	1.7	26
Al mudstone	3.2	2463	3.94	2.6	1.7	1.6	25
Quartz sandstone	2	2500	3.68	2.15	1.5	1.12	28
Lower rock mass	8.4	2695	5.2	4.1	3.3	2.12	35

model uses an elastoplastic constitutive model, and the failure criterion uses the Mohr–Coulomb criterion. See the first section for the loading schemes.

The principal stress difference and plastic zone distribution nephogram of the surrounding rock under different stress lode angles are shown in Figure 4: (1) in the σ_v type stress field, as the stress lode angle increases, the plastic zone of the surrounding rock increases first and then decreases. When $\theta \leq 50^\circ$, the damage range of surrounding rock is mainly concentrated in the surrounding rock of the roof, floor, and shoulder; this is due to the large principal stress difference in the surrounding rock of the roof, floor, and shoulder. When $\theta = 70^\circ$, the shape of the plastic zone is approximately elliptical due to the uniform distribution of the principal stress difference; (2) in the σ_H type stress field, the plastic zone range of the surrounding rock of the roadway increases with the increase of the stress lode angles. When $\theta \leq 110^\circ$, the distribution of the principal stress difference is relatively uniform, and the shape of the plastic zone is approximately elliptical. As θ increases, the principal stress differences of the surrounding rock of the roof and floor decreases, and the principal stress differences of the surrounding rock of two side walls and shoulder increases, which results that the plastic zone gradually develops toward the deep surrounding rock and the plastic zone is in the shape of "butterfly". (3) In the σ_h type stress field, when θ is small, the principal stress difference of the surrounding rock of two side walls is greater than that of the surrounding rock of the roof and floor, and the plastic zones are mainly distributed in the surrounding rock of two side walls. As θ increases, the principal stress difference of the surrounding rock of the roof and floor is greater than that of the surrounding rock of two side walls, the range of the plastic zone of the surrounding rock of the roof and floor is gradually increasing. The numerical simulation calculation results show that the shape of the plastic zone of the surrounding

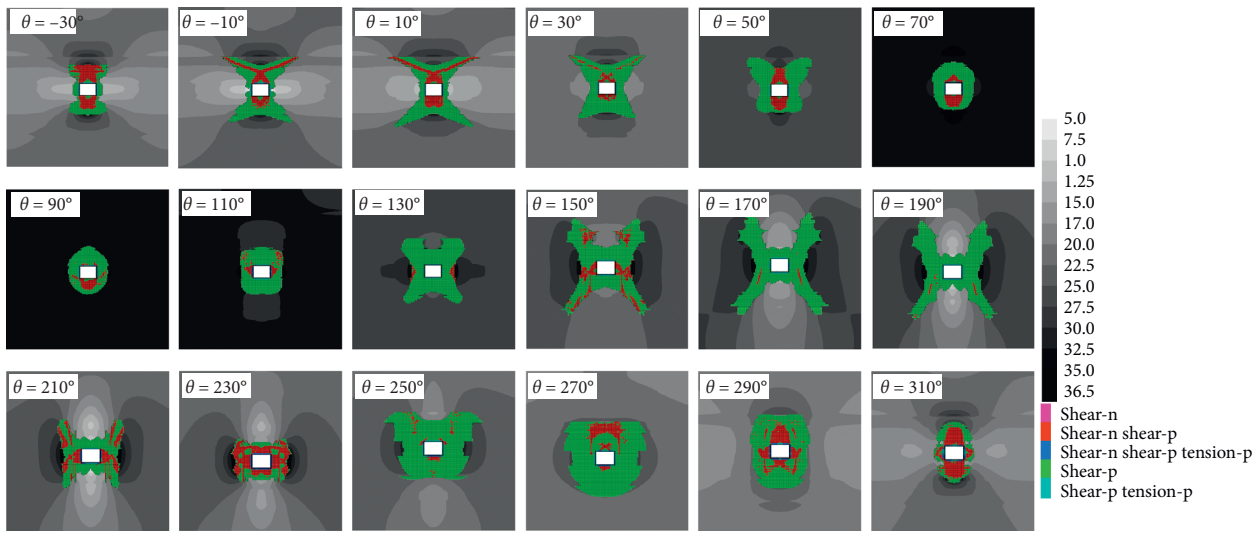

Figure 4: Principal stress difference and plastic zone distribution nephogram.

rock of the roadway under different stress lode angles is mainly round, oval, and "butterfly," and the shape and range of the plastic zone are closely related to the distribution of the principal stress difference which is consistent with the theoretical calculation results.

Under the condition of different stress lode angles, the variation law of the maximum value of principal stress difference in the surrounding rock of the roadway is shown in Figure 5. As shown in Figure 4, in the σ_v-type stress field, as the stress lode angle increases, the maximum value of the principal stress differences of the surrounding rocks of the roof and floor decreases linearly, while the change of the principal stress differences of the surrounding rocks of the roadway side walls is less affected by the stress lode, the variation is not large. With the increase of the stress lode angle, the maximum value of the principal stress difference between the roof, floor, and wall surrounding rock is approaching, and the stability of the surrounding rock of the roadway gradually increases; in the σ_H-type stress field, the variation of the principal stress difference between the surrounding rock of the roof and floor is small, while the principal stress difference of the surrounding rock of the wall increases with the increase of the stress lode angle, therefore, the larger the θ, the worse the stability of the surrounding rock of the roadway, and the more difficult the roadway support is; in the σ_h-type stress field, as θ increases, the principal stress difference of the surrounding rock of the roof and floor gradually decreases, and the principal stress difference of the surrounding rock of the wall gradually increases; under different stress lode angle conditions, the stability of different areas of the surrounding rock of the roadway is quite different.

3. The Crushing Gradient Effect of the Surrounding Rocks of the Roadway Affected by θ

After the excavation of deep surrounding rocks, the stress redistribution around the roadway will form a stress gradient. As shown in Figure 6, this stress gradient is a very important factor that causes the surrounding rocks of the roadway to break [23–26]. Under the action of the stress gradient field formed along the radial direction of the roadway, the degree of rock fragmentation along the radial direction of the roadway is different. Generally, the crack is densely developed near the roadway, and the crack width is large. The crack gradually becomes sparse and narrow outside, and the structural level variation appears, leading to structural gradient damage of the surrounding rocks.

In nature, engineering rock masses are often subjected to nonuniform loads across varying sizes. Nonuniform load will cause uncoordinated deformation at various points in the rock bodies. Tensile stress and rock mass damage often occur in areas with significant uncoordinated deformation zones. Therefore, this uncoordinated deformation is easy to cause rock mass degradation and instability. Microscopically, for polycrystalline materials such as rocks, heterogeneity is the main feature, and the general mineral particles are irregularly shaped, which can easily lead to stress concentration inside the rock. [27–29]. The increase of stress will lead to the thickening of the slip layer, and the coordination of mineral particles is difficult, and the structure cannot be rationally optimized, and the deformation is intensified, and the stress change occurring in a certain direction, that is, the stress gradients will lead to uneven distribution of deformation and failure to coordinate to cause plasticity destruction. Under the action of new mineral particle structure and stress gradients, the stress at the interface of mineral particles in some regions is high, but that in some regions is very low. Therefore, the force of the mineral particles is microscopically characterized by unevenness and anisotropy. Under the action of stress gradients, the heterogeneity of the rock mass itself is magnified, and the difference between the mineral particles and the deformation inconsistency is significant, which aggravates the fracture of the rock masses.

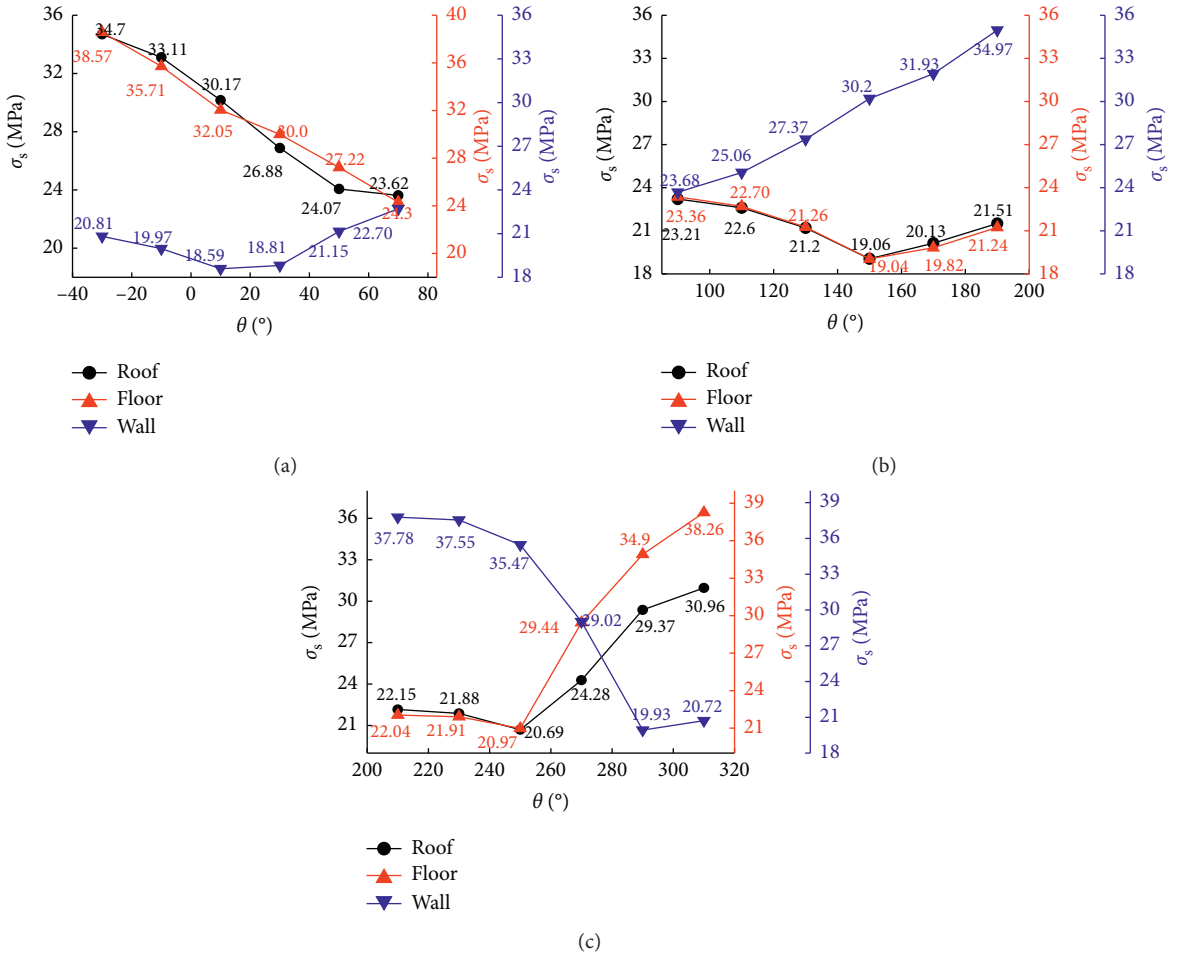

Figure 5: Evolution of the principal stress difference maxima. (a) σ_v-type stress field. (b) σ_H-type stress field. (c) σ_h-type stress field.

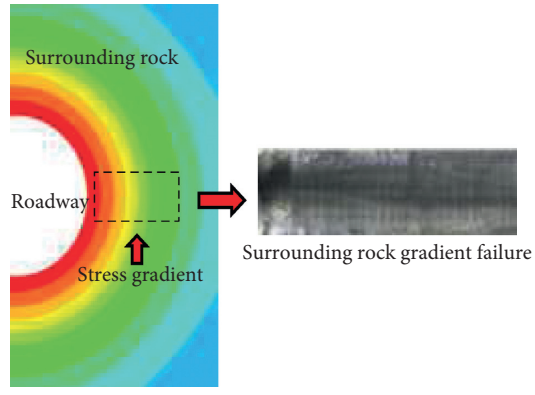

Figure 6: Schematic diagram of the surrounding rock failure of the roadway.

3.1. The Influence of Stress Gradient on Rock Mass Instability. In order to analyze the influence of stress gradients on the failure modes of coal rocks, based on the local load loading test device [6], the failure characteristics of coal samples under nonuniform load conditions are obtained, as shown in Figure 7. The average uniaxial compressive strength of the specimens was 40 MPa. The specimens were evenly divided into three regions: A, B, and C. During the loading process, a fixed load was first applied to the B region, and then, the load was applied to the C region until the specimen was broken. The A region was always 0 MPa. The experiment was divided into four groups, the load values of the B region were set to 2 MPa, 4 MPa, 6 MPa, and 8 MPa, respectively. The average ultimate strength values of the C region when the specimens

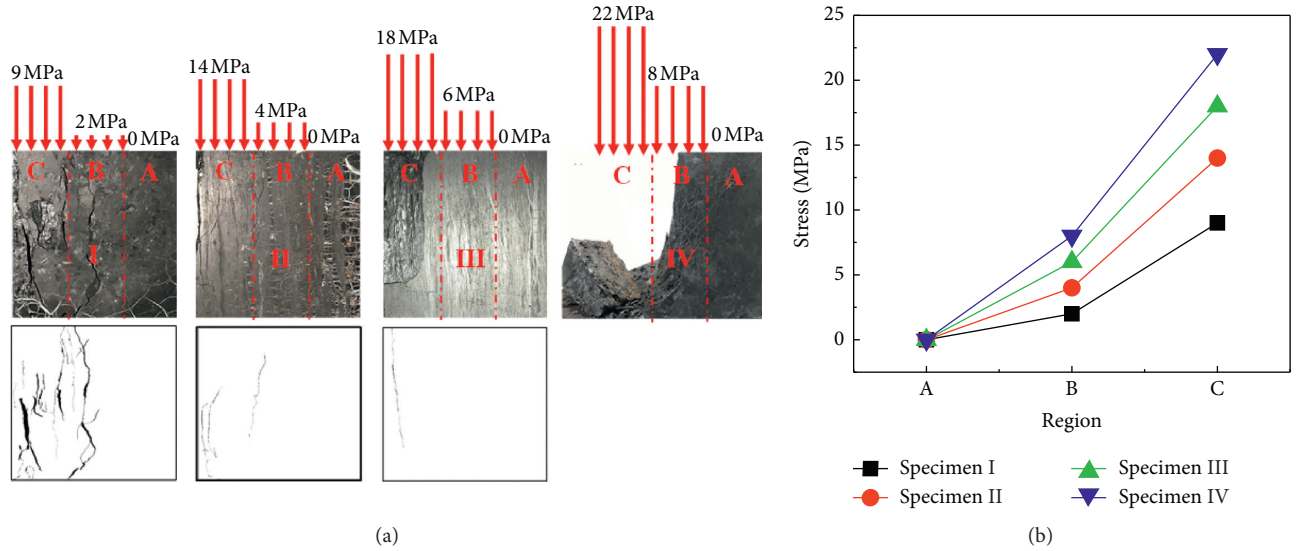

FIGURE 7: Influence of stress gradient on failure characteristics of coal rock. (a) Failure characteristics of the specimen. (b) Stress distribution in different regions.

were broken were 9 MPa, 14 MPa, 18 MPa, and 22 Mpa, respectively, as shown in Figure 7.

The surface crack distribution at the moment of the instability of the specimen under different loading conditions recorded by a high-speed camera and the corresponding crack sketch is shown in Figure 7(a). When the load value in the area C of the specimen was 22 MPa, the specimen suddenly burst. The specimen was severely broken, and the camera failed to capture the crack distribution before its instability. If the stress gradient of the specimen is characterized by the slope of each curve in Figure 7(b), the larger the stress gradient, the higher the strength of the specimen, and the more severe the failure.

In fractal rock mechanics, the box-counting dimension method uses different square grids ($\delta * \delta$) to cover the objects to be measured, to obtain the number $N(\delta)$ of square grids covering the objects under different sizes, and then calculates the fractal dimensions by the following formula:

$$\log N(\delta) = \log a - D \log \delta, \tag{12}$$

where δ is the square size; a is a constant; and D is the fractal dimension.

The MATLAB fractal dimension calculation program was used to identify and calculate the crack pictures in Figure 7(a). The calculation results are shown in Figure 8.

From the calculation results, it is known that the fitting degrees R^2 are all greater than 0.9, and the fitting effect is good, which indicates that the logarithm of the square size selected by the calculation program has a good linear relationship with the corresponding logarithm of the number of square grids covering the cracks. Under different stress gradients, the fractal dimension of cracks on the surface of coal samples is 1.11~1.46 and the fractal dimension of cracks decreases with increasing stress gradient. The fractal dimension is mainly positively related to the complexity of the crack and the crack bifurcation. Therefore, the greater the stress gradient, the lower the bifurcation frequency of crack propagation when the coal rock is unstable.

In summary, the greater the stress gradient, the higher the strength of the coal rock and the more severe the damage. Moreover, when the coal rock is unstable, the larger the stress gradient is, the lower the crack bifurcation frequency is, and the simpler the crack propagation form is.

3.2. Effect of Stress Lode Angle on Stress Gradient Distribution of Surrounding Rock of Roadway. In order to simplify the research, the stress gradient along the axial direction of the roadway is not considered. This paper mainly considers the radial stress gradient change of the surrounding rocks of a certain section of the roadway. Taking a section of the roadway, taking the rock masses near the roadway as the research object, because the rock masses near the roadway are damaged by the compression and friction of other rock masses, a region is selected in the place where the damage occurs, and a certain point O on the surface of the roadway is assumed as the point at which the destruction occurs. c is defined as the relative stress gradient at a point in the damage zone [30], the expression is as follows:

$$c = \left| \frac{\partial \sigma}{\partial r} \cdot \frac{1}{\sigma_0} \right|, \tag{13}$$

where r is the distance from a point in the zone of destruction to the point of failure O; $(\partial \sigma / \partial r)$ is the stress gradient at a point in the zone of failure; σ_0 is the stress value experienced by a failure point O near the roadway.

Define the weight function $\psi(l)$ to indicate the weight of the impact of a point in the damaged area on the destruction of the rock block. The weight function can be expressed as follows:

$$\psi(l) = 1 - cl(1 + \sin \alpha). \tag{14}$$

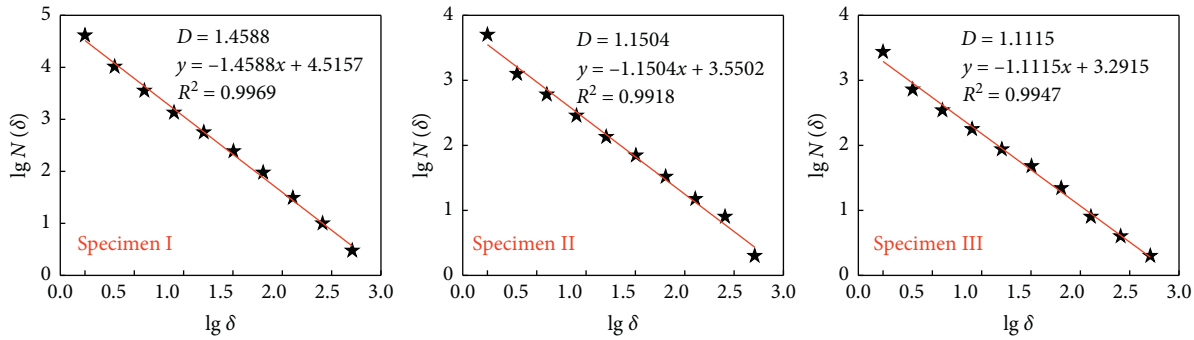

Figure 8: Calculation result of fractal dimension of crack.

There is a stress function that satisfies the mechanical characteristics of the rock block in this area. The average stress of the rock block can be expressed as follows [30]:

$$\overline{\sigma_i} = \frac{1}{S}\int_{\Omega} \varphi\left(\sigma_{ij}\right)\psi(l)\mathrm{d}s. \tag{15}$$

In the formula, S is the area of the failure area. Equation (15) shows that the failure of a rock block is not only related to the stress at the failure point but also to a certain range of stress fields.

According to the mechanical properties of the rock and the stress distribution of the surrounding rock of the roadway, the maximum principal stress of the surrounding rock is used to reflect the stress gradient of the surrounding rock, that is, let $\sigma = \sigma_1$. When studying the stress gradient and average stress distribution characteristics of the surrounding rock of the roadway in the radial direction, the formula (15) can be simplified, that is, only all the maximum principal stresses at a distance of l from the roadway are calculated. Then, the average maximum principal stress at l from the roadway is as follows:

$$\overline{\sigma_i} = \overline{\sigma_1} = \frac{1}{l}\int_{R_0}^{l} \sigma_1 \psi(l)\mathrm{d}l. \tag{16}$$

The average maximum principal stress takes into account the influence of the surrounding rock mass on a rock somewhere. The ratio of the average maximum principal stress to the maximum principal stress of the surrounding rock is called the stress compensation rate ν, that is, $\nu = (\overline{\sigma_1}/\sigma_1)$. For a point near the roadway (when $l = R_0$), $\sigma_0 = \sigma_1|_{r=R_0}$. Based on the above formula, taking the stress lode angle $\theta = 270^\circ$ as an example, the distribution law of the stress gradient, maximum principal stress, and stress compensation rate of the surrounding rock of the wall ($\alpha = 0^\circ$) is shown in Figure 9.

As shown in Figure 9, the closer to the roadway surface, the larger the stress gradient, the greater the change in the maximum principal stress, the lower the rock's stress compensation rate, and the surrounding rock prone to failure. The farther from the roadway, the smaller the stress gradient, the smaller the maximum principal stress value, the smaller the change range, the higher the stress compensation rate, and the more stable the surrounding rock. Based on the distribution characteristics of the stress gradient, the surrounding rock of the roadway is divided into three areas of I, II, and III. Among them, the stress gradient of the surrounding rock in area I is high and the surrounding rock is severely damaged. Region II is a transition region, and its surrounding rock stability is better than that of the region I. The stress gradient of surrounding rock in area III is low and the variation range is small, which is the stable area of surrounding rock of roadway.

Under different stress lode angle conditions, the stress gradient distribution characteristics of the roof and wall surrounding rock are shown in Figure 10. In the σ_v-type stress field, the stress gradient distribution of the surrounding rock of the roof is less affected by the stress lode angle, while the stress gradient distribution of the surrounding rock of the wall is greatly affected by the stress lode angle. In the σ_H-type stress field, the stress gradients of the wall surrounding rock and the roof surrounding rock both increase as the stress lode angle increases, and the stress gradient value of the roof surrounding rock is greater than that of the wall surrounding rock, indicating that the fragmentation of the roof surrounding rock is greater than that of the wall surrounding rock. In the σ_h-type stress field, the stress gradient value of the surrounding rock of the roof is generally greater than that of the surrounding rock of the floor, and the magnitude of the change in the stress gradient is greatly affected by the stress lode angle.

4. Roadway Support Measures considering the Influence of θ Change

(1) In the σ_v-type stress field, the shear stress (principal stress difference) of the surrounding rock of the roof and floor is larger, the surrounding rock damage range is greatly affected by the θ change, and the surrounding rock of the shoulder of the roadway is seriously damaged. Therefore, the surrounding rock of the shoulder can be regarded as a key part of the roadway. When supporting, comprehensive measures should be taken in time to control the development of key parts, avoiding large-scale instability of the surrounding rocks of the roadway caused by the expansion of the plastic zones. High-strength and high-rigidity support should be applied to the shoulder of the roadway. For example, long anchor cables or lengthened bolt

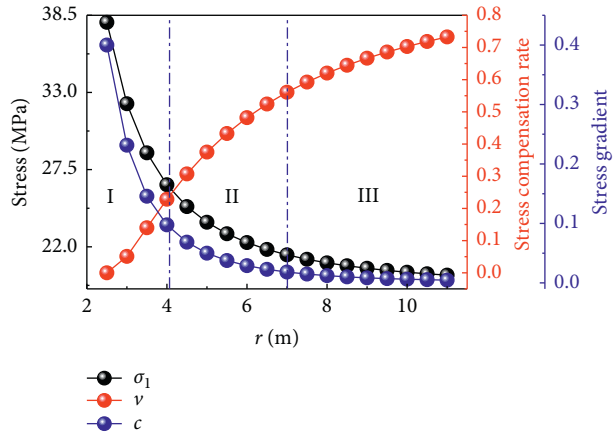

Figure 9: Distribution of stress gradient and stress compensation rate.

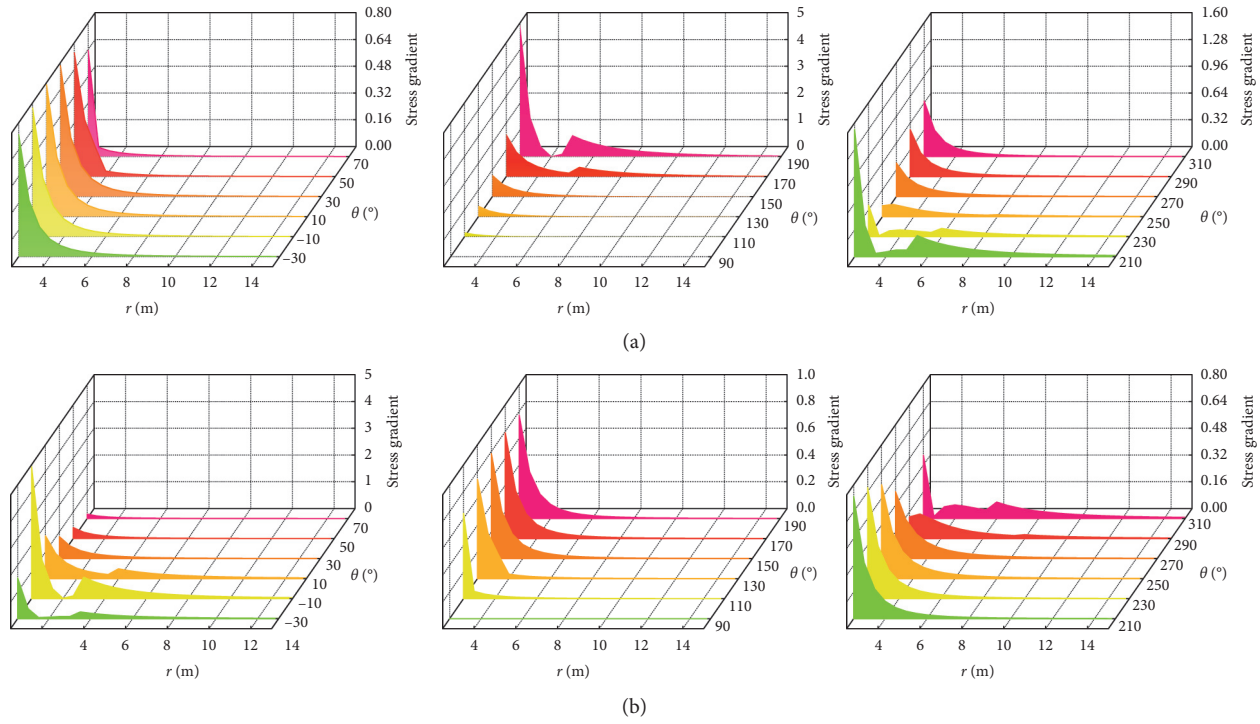

Figure 10: Stress gradient distribution of surrounding rock of roadway. (a) Roof. (b) Wall.

can be used to increase the support depth, so that the anchor cables (bolts) are anchored in the stable surrounding rocks. When θ is small, the shear stress of the surrounding rocks of the roof is large, which requires high strength and rigidity of the roof bolts (cables). The bolt stiffness is inversely proportional to the length of the bolt and is proportional to the cross-sectional area of the bolt [31, 32]. Therefore, under the premise that the bolt can be anchored in the stable rock masses, the length of the bolt should be reduced as much as possible. A high-strength bolt with a big diameter should be adopted. In addition, when θ is small, the stress gradient value of the surrounding rock of the floor is large, and the degree of fragmentation of the surrounding rock is high, care should be taken to protect the surrounding rock of the roadway.

(2) In the σ_H-type stress field, the surrounding rock failure range and stress gradient of the roadway increases with the increase of θ, and the damage depth of the surrounding rocks of the shoulder is larger. During support, attention should be paid to the development of the key parts of the shoulder. When the θ is larger, the depth of the surrounding rocks of the shoulder is larger. At this time, the support depth and strength of the surrounding rocks of the shoulder and the roof should be increased. When the stress gradient and the damage depth of

the surrounding rocks of the shoulder are larger, the prestressed truss anchor cable can be considered to support the roof [33]. The anchor cables are inclined and pass the maximum shear stress area of the shoulder and are anchored in the stable rock layers, which can effectively suppress falling of the surrounding rocks of the shoulder. And the truss anchor cable can apply high prepressing force from the horizontal direction and the vertical direction so that the surrounding rock is in a three-direction stress state, and the self-supporting ability of the surrounding rocks is improved.

(3) In the σ_h-type stress field, the plastic zones of the surrounding rocks of the roadway is more evenly distributed, and the damage range is less affected by θ. When the stress gradient is large and the surrounding rocks are relatively broken, the support density of the roadway should be appropriately increased. The steel strip or steel plate with high rigidity and wide area should be used to connect the bolts or anchor cables to increase the bearing area and make the supporting structure form a point-to-face support system to increase the integral strength of the support. Compared with the σ_H-type stress field and the σ_v-type stress field, the surrounding rock of the roadway in the σ_h-type stress field is more stable and the support is less difficult.

5. Engineering Verification

5.1. Onsite Monitoring. Based on the foregoing, the change of the stress lode angle directly affects the distribution of the principal stress difference and stress gradient of the surrounding rock of the roadway, while the distribution of the principal stress differences affects the failure range of the surrounding rock and the distribution pattern of the plastic zones, and the magnitude of the stress gradients affects the degree of fragmentation of the surrounding rock. The above research results are now applied to the field analysis, and the coal mine involved in the case study is located in Huozhou City, Shanxi Province, China. The location of the test roadway is shown in Figure 11; the N102 headgate is perpendicular to the direction of the transportation contact roadway. The roadways adopt a rectangular section with a section size of 4.4 m ∗ 3.2 m. The parameters of the supports of the two roadways are identical. Both sides of the N102 headgate are solid coals, and there is no geological structure near this section. This section has not been mined, so the N102 headgate and the transportation contact roadway are not affected by mining.

It can be seen from Figure 11 that the degree of damage of the surrounding rock of the N102 headgate and the transportation contact roadway is quite different. The deformation and damage of the surrounding rock of the N102 headgate are serious, the rock fragmentation scale is small, and the deformation of the anchor plates and the tear of the nets are more common. The integrity of the surrounding rock of the transportation contact roadway is relatively good. Since there is no geological structure at the location of the N102 headgate and the transportation contact roadway, and the roadway is not affected by the mining; it can be preliminarily determined that the difference between the roadway direction and the principal stress direction (the stress lode angle of the surrounding rock of the roadway is different) is the main factor leading to the difference in the integrity of the surrounding rock of the roadway. According to the in-situ stress test data provided by the mine corporation, the maximum principal stress in this mining area is 21.1 MPa, which is approximately parallel to the direction of the N102 headgate; the intermediate principal stress is 16.3 MPa, which is vertical stress; the minimum principal stress is 7.4 MPa, which is approximately vertical to the direction of the N102 headgate. From equations (1) to (3), it can be seen that the stress lode angles of the N102 headgate and the transportation contact roadway are close to 130° and 290°, respectively. From the peeping results of the internal crack development of the surrounding rock in the roadway (Figure 12), the fracture depth of the surrounding rock of the N102 headgate is slightly larger than that of the transportation contact roadway. The fracture depth of the surrounding rock of the roof and the wall is not much different. The surrounding rocks of the shoulder of the N102 headgate have a relatively large depth of damage, the damage boundary of the surrounding rock of the transportation contact roadway is approximately elliptical, and the failure boundary of the N102 headgate is approximately "butterfly," which is consistent with the conclusions drawn in Figures 3 and 4.

From Figure 10, it is known that the stress gradient of the surrounding rock of the N102 headgate ($\theta = 130°$) is greater than that of the transportation contact roadway ($\theta = 290°$). Therefore, it is preliminarily determined that the difference in the degree of fragmentation of the surrounding rock between the N102 headgate and the transportation contact roadway is caused by different stress gradients. In order to obtain the actual distribution of the stress gradient of the surrounding rock in the N102 headgate and the transportation contact roadway, the vertical stresses of the five measuring points in the surrounding rock near the shoulder corners of the two roadways were monitored. The location of the stress sensors is increased from 1 m to 5 m along the radial direction of the roadway, and the horizontal distance of these sensors along the roadway is 0.8 m, as shown in Figure 13(a).

The vertical stress monitoring results of the surrounding rock of the two roadways are shown in Figure 13(b). The borehole stress meters can only measure the relative value of the vertical stress of the surrounding rock, but not its absolute value. The measured stress value is smaller than the absolute stress value, but it can reflect the approximate distribution of the vertical stress of the surrounding rock. The measured vertical stress value is linearly fitted, and the slope of the fitted curve is used to represent the stress gradient. From the test results, it is known that the vertical stress values of the N102 headgate and the transportation contact roadway at each measurement point are not much different, and the vertical stress gradient of the N102 headgate is slightly larger than that of the transportation

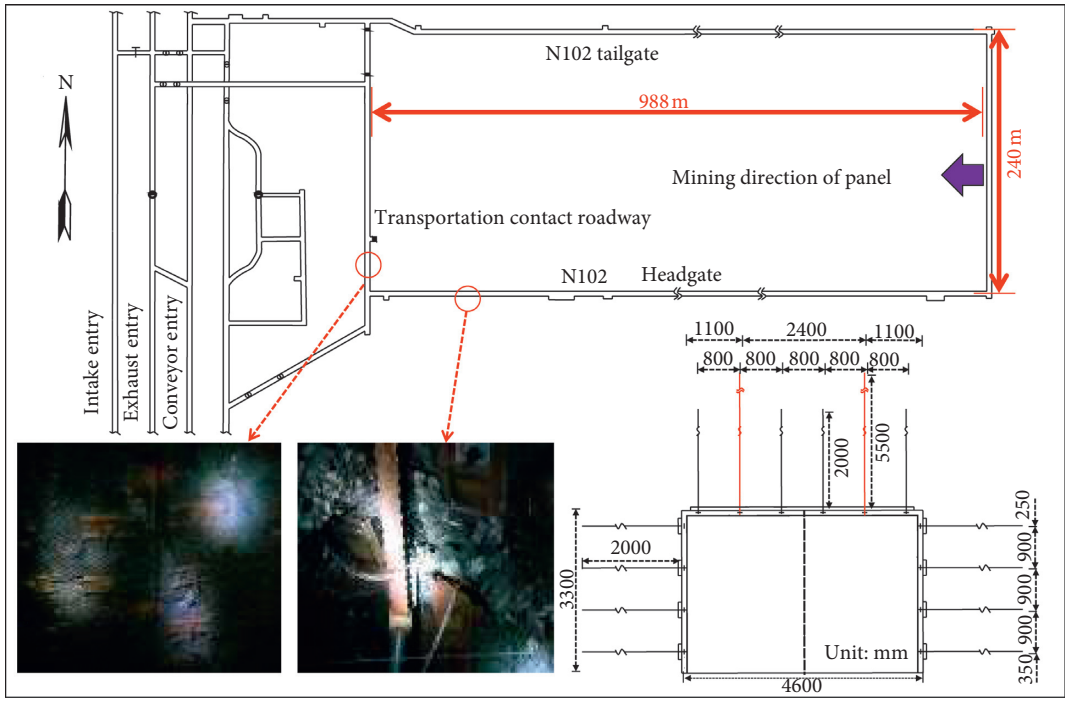

Figure 11: Location of test roadway.

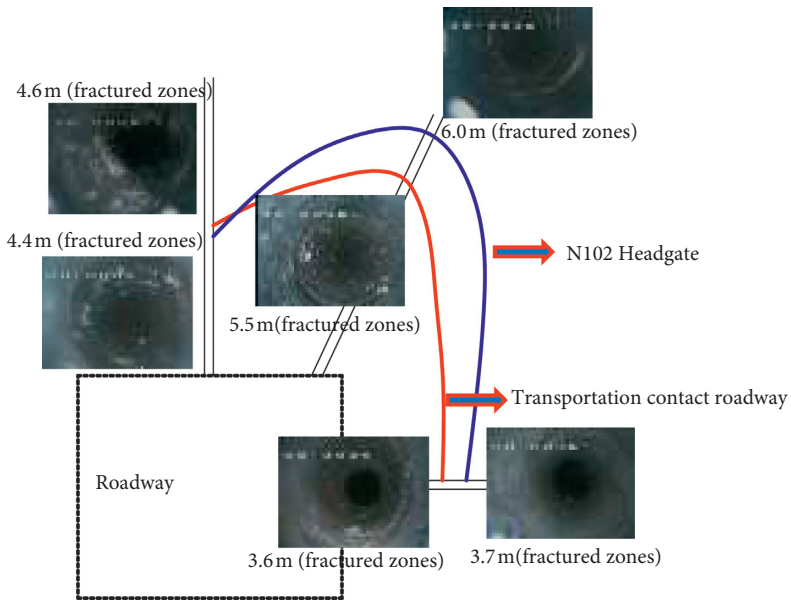

Figure 12: Drilling and peeping of the surrounding rock of the roadway.

contact roadway, which is consistent with the theoretical analysis result (Figure 10). Therefore, the different stress gradients are the main factors for the different degrees of fragmentation of the surrounding rock of the two roadways.

5.2. Support Measures Improvement. Based on the results of theoretical analysis and onsite observations, although the same support method was adopted for the N102 headgate and the transportation contact roadway, due to the different stress environments (stress lode angles), the plastic area of the surrounding rock of the transportation contact roadway is approximately elliptical, the damage range is small, and the stability is better. However, the plastic zone of the surrounding rock of the N102 headgate has a "butterfly" distribution, the damage depth of the surrounding rock at the shoulder of the roadway is large, and the stress gradient is large, and the surrounding rock is severely damaged, which results in the support failure phenomenon in the local area of the roadway. From the perspective of the destruction of the

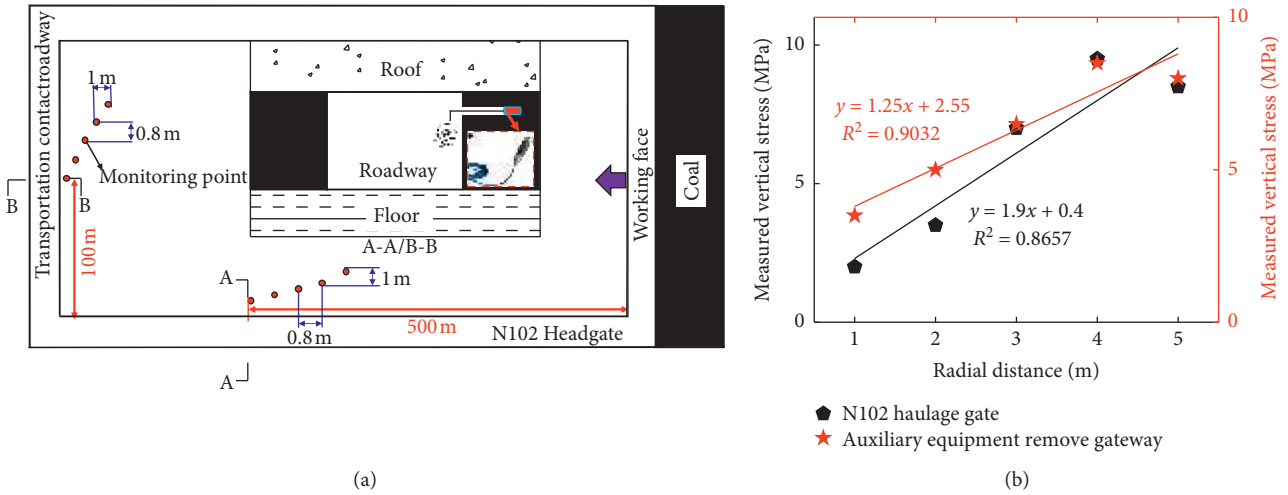

Figure 13: Layout of stress monitoring points and monitoring results. (a) Schematic layout of monitoring points (b) Monitoring results.

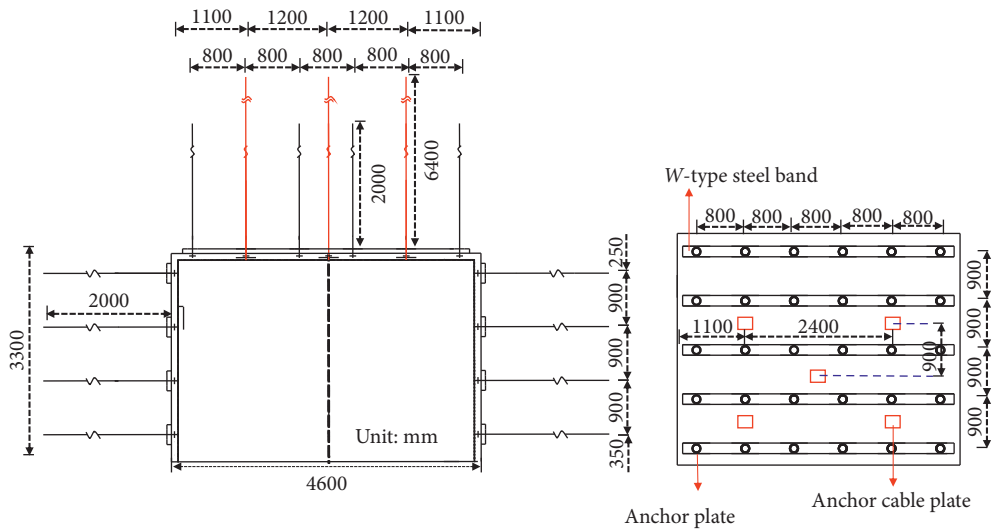

Figure 14: N102 headgate support scheme.

surrounding rock of the roadway, the original support scheme of the N102 headgate has the problems of low support density, short roof cable length, and unstable anchor foundation. The initial support scheme was modified to increase the support density and support depth of the original support scheme. The modified support scheme is shown in Figure 14. The roof and the two walls used 2 m long and 20 mm diameter steel bolts. The roof bolt spacing is 800 mm, the row spacing is 900 mm, and the gasket was changed to $W3 \times 280 \times 4350$ steel strip to increase the force area of the surrounding rocks; the spacing of the anchors of two walls is 900 mm and the row spacing is 800 mm. The bolts of the roof and two side walls of the roadway adopted a piece of CKb2340 resin anchoring agent and a piece of Z2360 resin anchoring agent separately, the total length is 1000 mm. The bolt pretightening torque is not less than 300 N·m. Aiming at the characteristics of larger damage depth and large stress gradient of the surrounding rock at the shoulder of the N102 headgate, the support density and depth of the roof are increased, and the row spacing of the anchor cables is adjusted to 2400×1800 mm, and the "2·1·2" arrangement was adopted, that was, one anchor cable was added between every two rows of anchor cables. The anchor cable adopted the steel strand with a diameter of 18.9 and a length of not less than 6200 mm (the specific length was adjusted according to the change of the site stratigraphic horizon in time). Two pieces of CKb2340 resin anchoring agent and Z2360 resin anchoring agent were selected, and the pretightened force of the anchor cable was not less than 200 kN.

In order to ensure that the support scheme is feasible, the measuring points were set in the roof and walls of the N102 headgate, and the deformation of the surrounding rock of the roadway after the modification of the support scheme was monitored, as shown in Figure 15. The field monitoring results show that the deformation rate of the surrounding

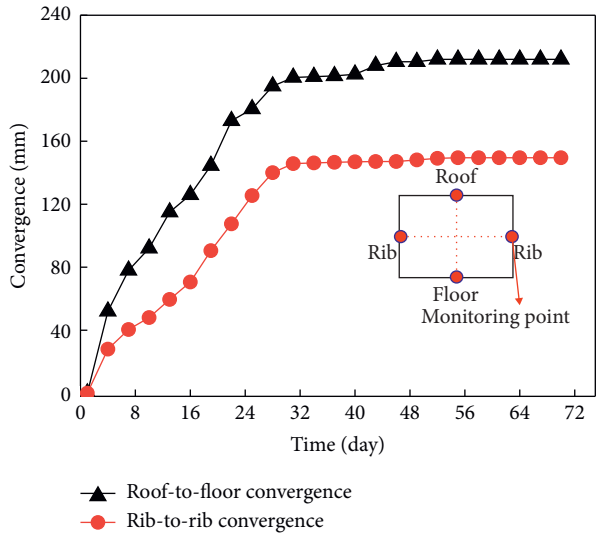

Figure 15: Monitoring results of surrounding rock deformation of roadway.

rock in the first 25 days is relatively large, and the deformation of the surrounding rock tends to be stable in days 25~35. The maximum displacement of the roof and floor is 210 mm, and the maximum displacement of the wall is 150 mm. The surrounding rock control effect is good. During the mining of 102 working faces, the deformation of the roadway increased significantly. At the 10 m in front of the working face, the maximum displacement of the roof and floor is 460 mm, and the displacement of the wall is 380 mm, meeting the needs of pedestrians, ventilation, and transportation.

6. Conclusions

(1) Based on the distribution of the stress lode angle, the stress of the surrounding rock of the roadway is divided into σ_v-type stress field, σ_H-type stress field, and σ_h-type stress field. Under different stress lode angle conditions, the distribution of the principal stress difference of the surrounding rock of the roadway is quite different, and the distribution of the principal stress difference has a direct effect on the shape and scope of the plastic zone of the surrounding rock of the roadway. In the σ_v-type stress field and the σ_H-type stress field, the shape of the plastic zone of the surrounding rock of the roadway is mainly oval and "butterfly," while in the σ_h-type stress field, the stress lode angle has little effect on the range of the plastic zone. The shape of the surrounding rock plastic zone is mainly oval.

(2) The stress gradient has an important effect on the damage degree of the surrounding rock of the roadway. The larger the stress gradient, the higher the strength of the rock mass and the more severe the damage. The change of the stress lode angle has a great influence on the stress gradient distribution law of the surrounding rock of the roadway. In the σ_v-type stress field, the stress gradient distribution of the surrounding rock of the roof is less affected by the stress lode angle, while the stress gradient distribution of the surrounding rock of the wall is greatly affected by the stress lode angle; in the σ_H-type stress field, the stress gradients of the wall surrounding rock and the roof surrounding rock both increase as the stress lode angle increases, and the stress gradient value of the roof surrounding rock is greater than that of the wall surrounding rock; in the σ_h-type stress field, the stress gradient value of the surrounding rock of the roof is generally greater than that of the surrounding rock of the floor, and the magnitude of the change in the stress gradient is greatly affected by the stress lode angle.

(3) Under different surrounding rock stress environments, the focus of roadway support should be different. In type σ_v and type σ_H stress fields, the surrounding rock of the shoulder of the roadway is seriously damaged. Therefore, the surrounding rock of the shoulder can be regarded as a key part of the roadway. During support, attention should be paid to the development of the key parts of the shoulder. In the σ_h-type stress field, the plastic zones of the surrounding rocks of the roadway is more evenly distributed, and the damage range is less affected by θ.

(4) The effect of the stress lode angle on the stability of the surrounding rock of the roadway was verified in the field, two roadways with the same supporting parameters and cross-sections (N102 headgate and transportation contact roadway) were selected for observation. Both roadways are not affected by the mining and are perpendicular to each other. The field observation results show that the plastic zone morphology, failure depth, and fragmentation of the surrounding rock of the N102 headgate and transportation contact roadway are quite different. The field monitoring results and theoretical calculations of the surrounding rock failure range and stress

gradient distribution are relatively consistent; the stress lode angles of the two roadways are 130° and 290°, respectively. The difference of the stress lode angles is the main factor for the large difference in the stability of the surrounding rock of the two roadways.

Data Availability

The relevant data of this article are included within the manuscript.

Conflicts of Interest

The authors declare that they have no conflicts of interest.

Acknowledgments

The authors gratefully acknowledge the financial support of The Open Fund Project of State Key Laboratory of Mining Response and Disaster Prevention and Control in Deep Coal Mines (SKLMRDPC19KF01), National Science Fund Subsidized Project (51474220), and Basic Scientific Research Project of the CPC Central Committee (no. 2009QZ03).

References

[1] M. He and H. Xie, "Study on mechanics in deep mining engineering," *Chinese Journal of Rock Mechanics and Engineering*, vol. 24, no. 16, pp. 2803–2813, 2005.

[2] K. Wang and F. Du, "Coal-gas compound dynamic disasters in China: a review," *Process Safety and Environmental Protection*, vol. 133, pp. 1–17, 2020.

[3] H. E. Fu-lian and G. Zhang, "Stability analysis and control of deep underground roadways subjected to high horizontal tectonic stress," *Journal of China University of Mining & Technology*, vol. 44, no. 3, pp. 466–476, 2015.

[4] L. Jiang, A. Sainoki, H. S. Mitri, N. Ma, H. Liu, and Z. Hao, "Influence of fracture-induced weakening on coal mine gateroad stability," *International Journal of Rock Mechanics and Mining Sciences*, vol. 88, pp. 307–317, 2016.

[5] H. Zhao, G. Hu, F. Wang et al., "Quantitative analysis of crack expansion in specimens of coal having a single pre - existing hole," *Journal of China Coal Society*, vol. 42, no. 4, pp. 860–870, 2017.

[6] H. Zhao, G. Hu, M. Zhang et al., "Quantitative analysis of crack propagation in specimens of porous media having a borehole under local load," *Journal of China University of Mining & Technology*, vol. 46, no. 2, pp. 312–320, 2017.

[7] F. Du, K. Wang, X. Zhang, C. Xin, L. Shu, and G. Wang, "Experimental study of coal-gas outburst: insights from coal-rock structure, gas pressure and adsorptivity," *Natural Resources Research*, vol. 29, no. 4, pp. 2481–2493, 2020.

[8] S. Zhang, S. Li, H. Xiao et al., "Surrounding rock principal stress difference evolution law and control of gob-side entry driving in deep mine," *Journal of China Coal Society*, vol. 40, no. 10, pp. 2355–2360, 2015.

[9] W. Zhao, L. Han, Y. Zhang et al., "Study on the influence of principal stress on the stability of surrounding rock in deep soft rock roadway," *Journal of Mining & Safety Engineering*, vol. 32, no. 3, pp. 504–510, 2015.

[10] X. Yang, H. Jing, K. Chen et al., "Study on influence law of in-situ stress in deep underground rock on the size of failure zone in roadway," *Journal of Mining & Safety Engineering*, vol. 30, no. 4, pp. 495–500, 2013.

[11] M. Chen, W. Lu, C. Zhou et al., "Influence of initial in-situ stress on blasting-induced cracking zone in tunnel excavation," *Rock and Soil Mechanics*, vol. 30, no. 8, pp. 2254–2258, 2009.

[12] F. T. Wang, C. Zhang, S. F. Wei, X. G. Zhang, and S. H. Guo, "Whole section anchor–grouting reinforcement technology and its application in underground roadways with loose and fractured surrounding rock," *Tunnelling and Underground Space Technology*, vol. 51, pp. 133–143, 2016.

[13] H. Kang, B. Yi, F. Gao, and H. Lv, "Database and characteristics of underground in-situ stress distribution in Chinese coal mines," *Journal of China Coal Society*, vol. 44, no. 1, pp. 23–33, 2019.

[14] P. S. Lang, A. Paluszny, M. Nejati, and R. W. Zimmerman, "Relationship between the orientation of maximum permeability and intermediate principal stress in fractured rocks," *Water Resources Research*, vol. 54, no. 11, pp. 8734–8755, 2018.

[15] S. Senent, R. Jimenez, and A. Reyes, "Numerical simulation of the influence of small-scale defects on the true-triaxial strength of rock samples," *Computers and Geotechnics*, vol. 53, pp. 142–156, 2013.

[16] F. Du and K. Wang, "Unstable failure of gas-bearing coal-rock combination bodies: insights from physical experiments and numerical simulations," *Process Safety and Environmental Protection*, vol. 129, pp. 264–279, 2019.

[17] C. Xin, F. Du, K. Wang et al., "Damage evolution analysis and gas–solid coupling model for coal containing gas," *Geomechanics and Geophysics Geo-Energy and Geo-Resources*, vol. 7, p. 7, 2021.

[18] J. Lu, G. Yin, X. Li et al., "Deformation and CO_2 gas permeability response of sandstone to mean and deviatoric stress variations under true triaxial stress conditions," *Tunnelling and Underground Space Technology*, vol. 84, no. 2, pp. 259–272, 2019.

[19] J. Li, G. Yin, D. Zhang, X. Li, G. Huang, and H. Gao, "Mechanical properties and failure mode of sandstone specimen with a prefabricated borehole under true triaxial stress condition," *Geomechanics for Energy and the Environment*, vol. 25, Article ID 100207, 2021.

[20] Y. Li, "A simplified model of triaxial stress field around long openings," *Journal of China Coal Society*, vol. 4, no. 12, pp. 74–80, 1982.

[21] M. Kumruzzaman and J.-H. Yin, "Influences of principal stress direction and intermediate principal stress on the stress-strain-strength behaviour of completely decomposed granite," *Canadian Geotechnical Journal*, vol. 47, no. 2, pp. 164–179, 2010.

[22] F. He, X. Wang, L. Xu et al., "Principal stress difference transfer law and support in large-section open-off cut," *Rock and Soil Mechanics*, vol. 35, no. 6, pp. 1703–1710, 2014.

[23] J. A. Araújo, G. M. J. Almeida, J. L. A. Ferreira, C. R. M. da Silva, and F. C. Castro, "Early cracking orientation under high stress gradients: the fretting case," *International Journal of Fatigue*, vol. 100, pp. 611–618, 2017.

[24] N. Gates and A. Fatemi, "Notch deformation and stress gradient effects in multiaxial fatigue," *Theoretical and Applied Fracture Mechanics*, vol. 84, pp. 3–25, 2016.

[25] M. A. Antunes, C. R. M. da Silva, E. M. F. do Rêgo, and A. C. de Oliveira Miranda, "Stress intensity factor solutions for fretting fatigue using stress gradient factor," *Engineering Fracture Mechanics*, vol. 186, pp. 331–346, 2017.

[26] S. de Oliveira Miranda, G. Fortese, C. Ronchei, and D. Scorza, "A stress gradient approach for fretting fatigue assessment of metallic structural components," *International Journal of Fatigue*, vol. 101, pp. 1–8, 2017.

[27] L. Chang, H. Konietzky, and T. Frühwirt, "Strength anisotropy of rock with crossing joints: results of physical and numerical modeling with gypsum models," *Rock Mechanics and Rock Engineering*, vol. 52, no. 7, pp. 2293–2317, 2019.

[28] J. Lee and J. W. Hong, "Morphological aspects of crack growth in rock materials with various flaws," *International Journal for Numerical and Analytical Methods in Geomechanics*, vol. 43, no. 10, pp. 1854–1866, 2019.

[29] S.-Q. Yang, P.-F. Yin, Y.-H. Huang, and J.-L. Cheng, "Strength, deformability and X-ray micro-CT observations of transversely isotropic composite rock under different confining pressures," *Engineering Fracture Mechanics*, vol. 214, pp. 1–20, 2019.

[30] W. Yao, *Fatigue Life Prediction of structures*, pp. 153–157, National Defense Industry Press, Beijing, China, 2003.

[31] H. Kang, "Sixty years development and prospects of rock bolting technology for underground coal mine roadways in China," *Journal of China University of Mining & Technology*, vol. 45, no. 6, pp. 1071–1081, 2016.

[32] X. Feng, N. Zhang, and Z. Wen, "Mechanical responses and acoustic emission properties of bolting system under short encapsulation cyclic thrust tests," *International Journal of Fatigue*, vol. 121, pp. 39–54, 2019.

[33] L. I. Guichen, N. Zhang, Z. Liu et al., "Prestress truss bolt support technology for coal roadway," *Journal of Mining & Safety Engineering*, vol. 24, no. 2, pp. 150–154, 2007.